Meteorol. Z. (Contrib. Atm. Sci.), Vol. **30**, No. 2, 185–200 (published online February 5, 2021)

Mesoscale wind patterns over the complex urban terrain around Stuttgart investigated with dual-Doppler lidar profiles

Niklas Wittkamp[1*], Bianca Adler[1,2,3], Norbert Kalthoff[1] and Olga Kiseleva[1]

[1]Institute of Meteorology and Climate Research, Karlsruhe Institute of Technology, Germany
[2]Current affiliation: CIRES, University of Colorado, Boulder, CO, USA
[3]Current affiliation: NOAA Physical Sciences Laboratory, Boulder, CO, USA

(Manuscript received January 31, 2020; in revised form August 31, 2020; accepted November 13, 2020)

Abstract

The flow in the atmospheric boundary layer (ABL) over cities is crucial for the urban climate as it controls the exchange of heat, moisture and pollutants within the ABL and with the surroundings. In particular for cities in mountainous terrain, the mesoscale flow shows a high spatial and temporal variability, which poses great challenges to the means of observation. We used the dual-Doppler lidar scan strategy of virtual towers (VT), to measure profiles of the horizontal wind in the ABL over the city of Stuttgart in southwestern Germany. To study the mesoscale variability of the horizontal wind, we placed six VTs in the topographically structured investigation area, which is characterised by a basin-shaped valley opening into a major valley. Comparisons with radiosonde data show that reliable wind information can be retrieved from the VT measurements after careful processing. A statistical analysis reveals a strong dependence of the flow in the valleys below ridge height on the bulk Richardson number (BRN). A critical BRN of 1.25 is identified for the area, below which the flow below ridge height is dynamically unstable and coupled to the ambient flow above. For BRNs greater than 1.25, the flow is dynamically stable and the flow below ridge height is dominated by thermally driven down-valley winds, which are decoupled from the ambient wind. This study shows that the VT technique is applicable in highly complex terrain and a promising tool for the investigation of the flow in areas which are difficult to access by traditional in situ or single lidar measurements, like complex urban terrain.

Keywords: virtual towers, thermally driven circulation, bulk Richardson number, atmospheric boundary layer, wind field, urban climate under change – [UC]^2

1 Introduction

Cities located in mountainous terrain often suffer from bad air quality, as the exchange of heat, moisture and pollutants in the urban atmospheric boundary layer (ABL) and with the surroundings is limited (e.g. Wanner and Hertig, 1984; Mayer, 1999). The flow in the urban ABL is a complex superposition of processes on different scales, ranging from synoptic scale pressure systems over mesoscale topographic and thermal effects to microscale influences from buildings and human activities (Steyn et al., 2013). The pollutant distribution in urban valleys may strongly depend on the valley width and dimension (Rendón et al., 2020).

Atmospheric processes and flow over urban areas in mountainous terrain have been investigated previously in field experiments and numerical model studies. Steyn et al. (1997) found a complex circulation in the urban ABL in the Lower Fraser Valley in the USA, which was influenced by interactions between the close-by sea, mountains and the city, distributing Ozone and pollutants in the area. In the Salt Lake City Valley in the USA (e.g. Allwine et al., 2002; Lareau et al., 2013), a complex flow in the ABL was detected, resulting from a superposition of influences from the Great Salt Lake, the valley and the synoptic situation. Kuttler et al. (1998) analysed the cold air ventilation of the Cologne bay in western Germany during calm summer nights and observed an interaction between regional and microscale circulations controlling the degree of ventilation of cities in the area. In the Upper Rhine Valley in Germany, Kalthoff et al. (1998) and Kossmann et al. (1998) found that the structure of the convective boundary layer (CBL) is strongly influenced by the terrain and the CBL height has a dominating effect on the dispersion of pollutants. Klaus et al. (2003) investigated influences on the surface wind directions in the "Baar" mountain basin in southwestern Germany, where they found that the valley-like topographic structure leads to a predominance of dynamically forced channelling during the day and thermally driven channelling during nighttime. While all these studies examined ABL processes above and around cities located in broad valleys of widths on the order of 20 km and more, the number of studies in narrow, densely populated valleys is much smaller. Piringer and Baumann (1999) investigated how temperature changes related to an urbanized area affect the valley wind system in a narrow valley opening to the city of Graz in Austria. In the narrow

*Corresponding author: Niklas Wittkamp, Institute of Meteorology and Climate Research, Karlsruhe Institute of Technology, Germany, e-mail: niklas.wittkamp@partner.kit.edu

and deep Adige valley Giovannini et al. (2017) investigated fully developed diurnal mountain winds and found that inhomogeneities in the topographic structure as well as urban areas can modify diurnal up- and down-valley winds considerably.

In order to investigate the multi-scale processes which determine the structure and evolution of the urban ABL, comprehensive three-dimensional observations and highly resolved urban climate models, which are able to resolve whole cities down to single buildings, are essential. These models are also valuable tools for city planners in times of climate change and air pollution issues. A powerful urban climate model is the German model PALM-4U (Maronga et al., 2019), which has been developed within the large program $[UC]^2$ – Urban Climate Under Change, funded by the German Federal Ministry of Education and Research (BMBF) (Scherer et al., 2019b). To evaluate these kinds of models, intensive observations of the urban ABL are needed.

The possibilities of observing the wind field in the ABL by traditional in situ measurements are rather limited in urban areas, as finding suitable measurement locations and getting permissions is challenging and the spatial coverage of in situ measurements is usually sparse. However, cities are characterised by a very large spatial heterogeneity of surface conditions which demands a dense observation network. Even if in situ measurements are installed they only probe the lowest part of the ABL. The observational coverage of the upper part of the urban ABL is even worse and it remains underresearched (Barlow, 2014).

This gap can be closed using remote sensing techniques like Doppler lidar. From a single Doppler lidar horizontal wind profiles throughout the ABL can be retrieved using the velocity-azimuth display (VAD) or the Doppler beam swinging (DBS) technique (Werner, 2005). As these methods are based on the assumption of horizontally homogeneous flow, the accuracy of the retrieved wind profiles is rather limited over complex terrain (Bingöl et al., 2009). Considerably more accurate horizontal wind information can be retrieved by combining two Doppler lidar devices using the dual-Doppler method (Pauscher et al., 2016; Choukulkar et al., 2017). The dual-Doppler method was first applied to lidar measurements by Rothermel et al. (1985) and developed further in recent years. The dual-Doppler lidar method was used to study the mean (e.g. Newsom et al., 2005; Träumner et al., 2015) and the turbulent (e.g. Collier et al., 2005; Röhner and Träumner, 2013) flow over flat but inhomogeneous terrain.

Using the dual-Doppler lidar method vertical profiles of the horizontal wind can be obtained, with the so-called virtual tower (VT) scan technique (hereafter "wind" always refers to the horizontal wind unless otherwise stated). VTs are consecutive measurements of the wind at different heights along a profile. Calhoun et al. (2006) first used the VT technique to measure continuous profiles of the mean wind over Oklahoma City, a city in flat terrain in the USA. Damian et al. (2014) applied the VT technique to study a low-level jet (LLJ) over flat agricultural terrain in the wide Rhine Valley and found a good agreement of the VT measurements with measurements from a meteorological 200 m mast and a tethered-balloon probe. Newman et al. (2016) showed that the VT technique achieves better results than single profiling lidar measurements in homogeneous terrain in the Great Plains in the USA. The VT technique has considerable advantages over traditional in situ measurements: vertical profiles can be measured from close to the ground up to the top of the ABL or above, depending on the backscatter; VTs can be freely positioned within the limitations by the instrument setup geometry; they are applicable in densely built-up areas, as well as in complex terrain; and, as a remote sensing technique, they do not disturb the flow. However, to retrieve high-quality wind profiles from VT measurements a very high synchronisation of the scanning Doppler lidars is necessary and the retrieval requires a thorough quality control and careful processing. To get information on the horizontal distribution of the wind, several VTs have to be placed at different locations in the investigation area, which strongly increases the demands for the synchronization and the complexity of the scan pattern. While the VT technique is a very promising approach, it has to our knowledge not been used to study the three-dimensional distribution of the wind field over urban complex terrain.

In this study, the VT technique is used to investigate the flow characteristics in the – so far – little researched urban ABL in narrow, densely populated valleys. The target area is the city of Stuttgart in southwestern Germany. Stuttgart is a very good example for a large city located in mountainous terrain suffering from frequent air quality issues which are related to the complex topography (Mayer, 1999; Scherer et al., 2019a). This study focuses on the influence of the topography on meso-scale wind-field structures. Impacts on the microscale, i.e. individual buildings or street canyons are out of the scope of this investigation.

Three objectives are addressed in this study, with the first one being more technical:

1. Is it possible to use the VT method to derive mesoscale flow characteristics in the ABL in highly complex urban terrain? What processing steps are necessary?

2. What flow characteristics do occur in the ABL near Stuttgart and how are they affected by the topography?

3. How does the flow depend on ambient wind and atmospheric stratification?

To answer these questions, intensive measurements conducted in and around Stuttgart within the $[UC]^2$ programme were used. Besides the development of the urban climate model PALM-4U, the program aimed to gather comprehensive three-dimensional observational

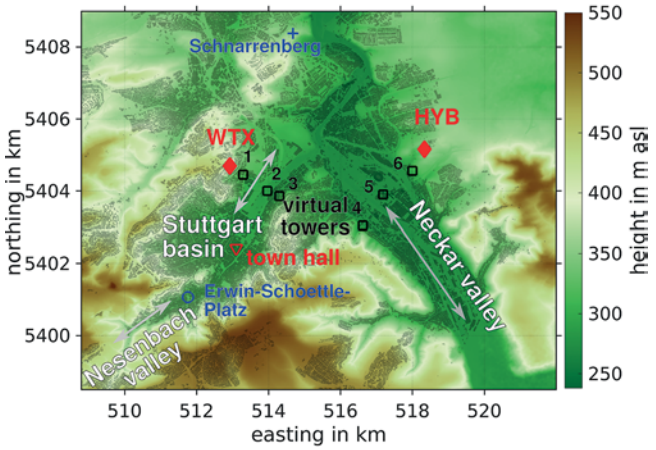

Figure 1: Terrain height (colour shading), buildings (grey shading) and locations of measurement sites in and around the city of Stuttgart: Doppler lidars for virtual towers (VT): WTX and HYB; profiling Doppler lidar (Windcube, WC) and microwave radiometer (MWR) on top of the town hall; radiosondes were launched from Erwin-Schoettle-Platz; meteorological station with near-surface and ceilometer measurements at Schnarrenberg. Arrows indicate the general orientation of the valleys. Topographic data provided by the German Aerospace Centre (DLR). Coordinate system: UTM (ETRS89) zone 32U.

data for process analyses and model validation and testing (Scherer et al., 2019a).

In the following section, the field campaign and the used instrumentation are described. The VT technique and the data processing are explained in Section 3. In Section 4, a case study under fair weather conditions is investigated in detail and in Section 5 a statistical analysis on the topographic influence is conducted. A summary and conclusions are given in Section 6.

2 Measurement setup and devices

2.1 Field campaign design

The data analysed in this study was gathered in the orographically structured area around the city of Stuttgart in southwestern Germany (Figure 1). The investigated area is characterised by the relatively broad Neckar valley (width ~2 km), which is orientated southeast-northwest, and a basin-shaped valley called Stuttgart basin ("Stuttgarter Kessel", ~3 × 3 km) which opens to the Neckar valley in the northeast. From the southeast the narrow Nesenbach valley joins the Stuttgart basin. The valley bottoms are at heights of 250–350 m above mean sea level (m asl), while the ridge height of the surrounding hills is about 520 m asl.

Three Doppler lidars and a microwave radiometer (MWR), which are part of the mobile integrated atmospheric observation platform KITcube (Kalthoff et al., 2013), were deployed in the area to measure wind, temperature and humidity (Figure 1, Kiseleva et al. 2019). Two Doppler lidars (WTX, HYB) were set-up on the slopes of the Neckar valley to measure profiles of the wind using the VT technique (Section 3.1). A third Doppler lidar (Windcube, WC) measured wind profiles in the Stuttgart basin, on the rooftop of the town hall in the city centre. The MWR was installed on top of the tower of the town hall, from which temperature and humidity profiles were derived. The instrument heights and measurement ranges of the devices are given in Table 1. Additional information on the ABL conditions were provided by Germany's National Meteorological Service (Deutscher Wetterdienst, DWD), which launched radiosondes at the Erwin-Schoettle-Platz during selected days and operates a meteorological station at Schnarrenberg, from where near-surface and ceilometer measurements are available.

Table 1: Locations of virtual towers (VT), Doppler lidars (WTX, HYB, WC) and microwave radiometer (MWR), topographic height (terrain plus building height) at the positions, and measurement height range. Coordinate System: UTM (ETRS89) zone 32U.

	easting (m)	northing (m)	topographic height (m asl)	height range (m asl)
VT 1	513 290	5 404 451	316	361–787
VT 2	513 963	5 404 000	287	339–2309
VT 3	514 299	5 403 861	302	347–787
VT 4	516 617	5 403 043	275	341–781
VT 5	517 182	5 403 903	316	303–2273
VT 6	517 996	5 404 559	301	333–773
WTX	512 924	5 404 697	392	(VTs)
HYB	518 332	5 405 157	357	(VTs)
WC	513 099	5 402 426	324	365–925
MWR	513 074	5 402 466	357	357–10 357

Doppler lidar measurements for VTs were carried out on 36 days in total, distributed over three periods from July to September 2017. During these days, measurements from the WC are available on 22 days, and MWR data are available on 17 days. For a 24-hour case study, radiosonde, ceilometer and near surface measurements are used additionally.

2.2 Doppler lidar devices

The two Doppler lidars (WTX, HYB) of the type "WindTracer", manufactured by Lockheed Martin, were used to derive wind profiles with the VT method (Section 3.1). Technical properties and settings of the two systems are given in Table 2 and are described in detail by Röhner and Träumner (2013) and Damian et al. (2014). For both devices, the range gate length was set to 69.5 m and the accumulation frequency was 10 Hz. The measurement range of the devices was 350 m to 12 km, depending on the atmospheric conditions. Both lidar systems are equipped with a freely configurable two-axis scanner. Software provided by the manufacturer makes it possible to perform highly synchronised scans with the two devices, which is required for VT measurements (Section 3.1).

Table 2: Technical properties and settings of the two "WindTracer" Doppler lidar devices WTX and HYB.

	WTX	HYB
laser type	Er:YAG	TM:LuAG
wavelength [µm]	1.617	2.023
pulse length [ns]	300	370
pulse energy [mJ]	2.7	2.0
pulse repetition frequency [Hz]	750	500
sampling rate [MHz]	250	250
accumulation frequency [Hz]	10	10
range gate width [m]	69.5	69.5

The third, vertically profiling Doppler lidar (WC) of the type "Windcube WLS8-3" manufactured by Leosphere, was used to get additional wind profiles. The device automatically determines wind profiles at its location, using the DBS technique. The device software calculates wind vectors in heights of 40–600 metre above the device in steps of 20 m at a temporal resolution of 10 min. The WC measured wind profiles in the centre of the Stuttgart basin, an area that was not covered by the VTs (Figure 1).

2.3 Additional instrumentation

An MWR manufactured by Radiometer Physics (humidity and temperature profiler "HATPRO") measured atmospheric microwave emission, from which temperature and humidity profiles were retrieved using an algorithm provided by the University of Cologne (Löhnert and Crewell, 2003; Löhnert et al., 2009). Details on the features of the device are given in Rose et al. (2005). The retrieval yields temperature profiles in vertical steps of 50 m close to the ground, increasing towards 200 m at the top of the ABL (Crewell and Löhnert, 2007). Potential temperature profiles were calculated from the retrieved temperatures using pressure profiles calculated from in situ pressure measurements at the device's housing with the barometric equation.

Vaisala "RS92" radiosondes were launched by the DWD at Erwin-Schoettle-Platz on selected days (Figure 1). Vertical profiles of pressure, temperature, relative humidity and wind speed and direction, are available throughout the troposphere with a vertical resolution of around 5–10 m.

At the meteorological station of the DWD at Schnarrenberg (Figure 1), standard near-surface meteorological variables such as temperature, pressure, humidity, precipitation and radiation are monitored. The data are available with a temporal resolution of 10 min. A ceilometer measuring attenuated backscatter was also operated at the station.

3 Method and processing

3.1 Dual-Doppler lidar and virtual towers

The principle of the dual-Doppler lidar method is to use two Doppler lidars to measure radial velocity at the same point in space and time, from two different positions. If the elevation angles ϕ of both lidar beams are small or the vertical wind component w can be neglected, the horizontal wind components can be calculated from the two radial velocities (equations e.g. in Damian et al., 2014). For non-zero vertical wind speeds and elevation angles, errors for the horizontal wind speed ΔU occur:

$$\Delta U = w \tan(\phi) \,. \tag{3.1}$$

Table 3: Errors in wind speed resulting from neglecting the vertical wind w in dependence of elevation angles ϕ. Errors calculated exemplarily for a horizontal wind speed of 5 m s^{-1} for typical values of w in the stable boundary layer (SBL) and the convective boundary layer (CBL) (Stull, 1988) and mean, median and maximum ϕ of the measurement layout. Relative values in brackets.

ϕ	SBL (w = 0.1 m s^{-1})	CBL (w = 2 m s^{-1})
8.4° (ϕ_{mean})	0.02 m s^{-1} (0.3 %)	0.30 m s^{-1} (5.9 %)
3.1° (ϕ_{median})	0.01 m s^{-1} (0.1 %)	0.11 m s^{-1} (2.1 %)
56.8° (ϕ_{max})	0.15 m s^{-1} (3.1 %)	3.05 m s^{-1} (61.1 %)

Error estimates for the applied measurement geometry due to non-zero elevation angles and vertical wind components are displayed in Table 3 for typical conditions in the stable boundary layer (SBL) and the CBL. While, on the average, errors are well below 10 % even in the CBL, where vertical wind speed can be large due to turbulence, maximum errors of around 60 % may occur for the largest elevation angles occurring at the tops of VT 2 and VT 5 (Figure 3 and Table 3). Terrain-following flow may also lead to a considerable vertical wind component. As this mainly occurs close to the ground where elevation angles are small (Figure 3), the resulting errors are expected to be small.

To minimize the effects of the propagation of individual lidar errors due to uncorrelated noise, the azimuthal intersection angle of the two lidar beams should be close to rectangular. Based on considerations of Stawiarski et al. (2013), Träumner et al. (2015) found intersection angles between 30° and 150° to be reasonable, which was considered for the measurement layout in this study.

The construction of VTs can generally be realised in two different ways: Calhoun et al. (2006) performed continuous intersecting range-height indicator scans, which result in a high temporal resolution, but low data accuracy due to missing synchronisation. Damian et al. (2014) used a synchronised stop-and-stare technique, where both lidars measured at discrete points in space simultaneously, for a certain amount of time. This technique results in a lower temporal resolution, but a higher spatial accuracy and data quality, and turbulent fluctuations can be measured or averaged out. An approach similar to the latter one was used in this study.

3.2 Measurement layout

In order to gain information on the horizontal as well as on the vertical variability of the wind field, six VTs

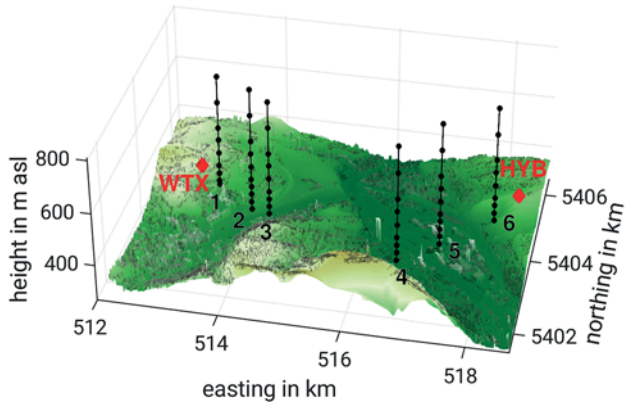

Figure 2: Arrangement of the six VTs with measurement heights (circles) over the topography. Measurement heights are displayed up to 800 m asl, the height axis is elongated by factor 5 relative to the horizontal axes. Terrain, buildings and coordinate system as in Figure 1.

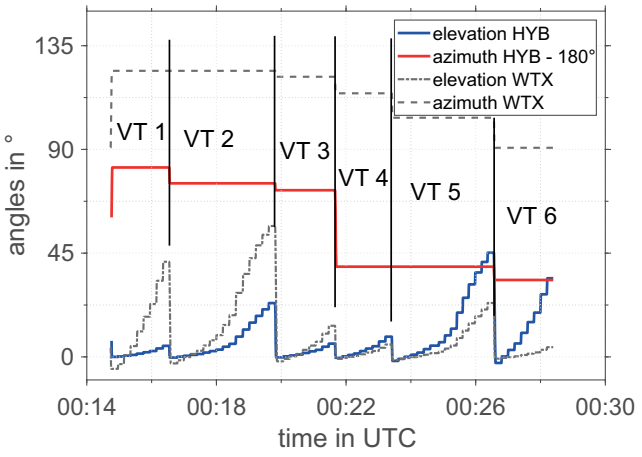

Figure 3: Lidar beam angles of both Doppler lidars during a complete scan cycle for VTs. Blue and red lines display elevation and azimuth angles of HYB (180° subtracted from azimuth for better visibility). Angles of WTX are displayed as dashed lines. Vertical black lines mark the boundaries of the time periods, during which the individual VTs are scanned.

were placed in the investigation area around Stuttgart, three across the opening of the Stuttgart basin to the Neckar valley (VTs 1–3), and three across the Neckar valley (VTs 4–6) (Figures 1, 2). Each VT consisted of 9 discrete measurement heights between 300 m asl and 800 m asl, with the lowest height 30–50 m above ground level (m agl) and with increasing vertical spacing upwards (Table 1 and Figure 2). The VTs in the middle of the valleys (VT 2 and VT 5) had 7 additional measurement heights up to 2300 m asl. The two lidar devices performed temporally synchronised scans, measuring simultaneously for 10 s at every measurement height of each tower, i.e. with an accumulation frequency of 10 Hz, 100 values are available at each height. The scan started from the lowest height of VT 1, proceeded upwards through all measurement heights of this tower, and continued with VT 2 to VT 6, scanning each tower from bottom to top (Figure 3). During the scanning of one VT, the azimuth angles stay constant while the elevation angles increase stepwise, with every step representing the 10 s measuring period at a specific height level. In total 68 heights were scanned and it took the two lidar devices approximately 15 min to complete one scan cycle. As the elevation angles of the lidars were relatively small for most measurement heights (85 % smaller than 22.5°), the errors resulting from neglecting the vertical wind component are assumed to be small for most cases (Figure 3 and Table 3).

3.3 Data processing

To retrieve high-quality profiles of the wind from the dual-Doppler measurements, several processing steps are necessary:

- *Identification of range gates for VTs.* Every measurement height of each VT is characterised by a unique combination of azimuth and elevation angle for the two Doppler lidars, given by its location in space (Figures 2, 3). For each lidar, the range gate closest in space to the specific measurement height was selected for the VTs.
- *Filtering of raw data.* The radial velocities measured by the two lidars at each measurement height were filtered in three steps in order to eliminate random noise and outliers before the calculation of the wind components: (i) A maximum radial velocity threshold filter of 15 m s^{-1} was applied to get rid of unrealistically high values. (ii) A minimum signal-to-noise ratio filter was applied to remove random noise caused by low backscatter signal. To keep as much data as possible a relatively low filter threshold was chosen. Due to different instrument specifications, different minimum signal-to-noise ratio thresholds were chosen (−8 dB for WTX and −7 dB for HYB). (iii) Remaining outliers were eliminated by setting a median absolute deviation threshold (e.g. Machiwal and Jha, 2012) for the radial velocities. Values exceeding a certain multiple of the median absolute deviation (6.7 for WTX and 6 for HYB) are regarded as outliers and filtered out. The filter was applied for each height for a (temporally) moving box containing 900 values at 10 Hz, i.e. roughly 1.75 h were taken into account. After the filtering 81 % of the raw data remained.
- *Calculation of wind vectors and temporal averaging.* The filtered radial velocities were averaged over each 10 s measurement interval and the horizontal wind components were calculated. The wind components were first calculated regardless of the number of values within the 10 s interval. If only very few values are available, strong fluctuations from one profile to the next and from one height to the other might occur. Removing periods during which less than 5 %, i.e. less than 5 out of 100 values, were

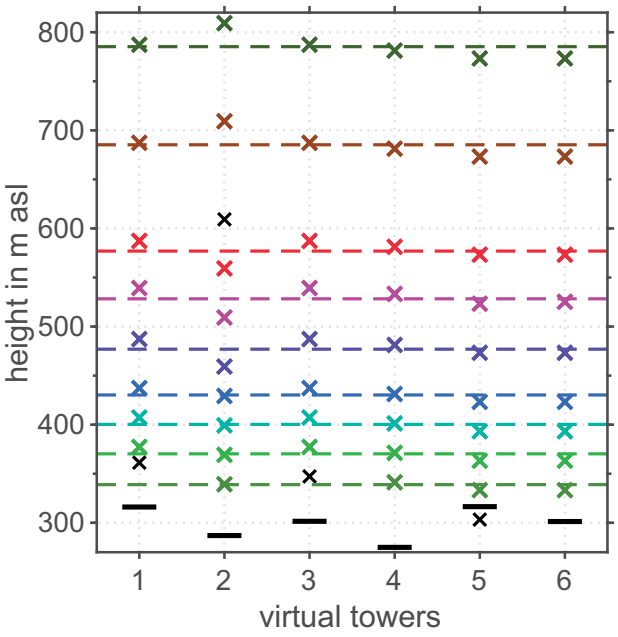

Figure 4: All nine common height levels of the six VTs. Coloured dashed lines mark the common height levels and actual measurement heights of all six VTs are displayed as crosses, with the same colour as the corresponding common height levels. Black crosses are measurement heights not assigned to any common height level. The lowest measurement heights were topographically disturbed at VT 1 and VT 3, and proved to be influenced by a tall building very close by at VT 5. Short black horizontal lines mark the topographic height (terrain height plus building height) at the respective VT position.

available, led to much more consistent and realistic wind profiles. After this availability filtering, 89 % of the original intervals remained. Due to the duration of one dual-Doppler scan the resolution of the resulting wind data is approximately 15 min. Variation of the flow within this interval cannot be covered by the measurement technique. Using the continuously measuring WC the uncertainty caused by assuming that a 10 s measurement represents a 15 min period can be estimated: At 405 m asl and 685 m asl, heights which are used in the subsequent analyses, the root-mean-square errors are 1.26 m s^{-1} and 1.46 m s^{-1}, with correlation coefficients of 0.79 and 0.85 (the values are based on data from the whole measurement campaign). While for the case study (Section 4) the 15-min data were used, the wind components were hourly averaged for the statistical analysis (Section 5). Note that only four to five samples were available for the hourly averages, which may cause a large uncertainty.

- *Determination of common height levels.* The actual measurement heights of the VTs were assigned for each VT individually before the campaign with respect to terrain height at the individual VT site. For the statistical analysis and to compare wind measurements at the different sites, common height levels in m asl are chosen for all VTs (Figure 4). The maximum distance of an actual height to the corresponding common height level is 24 m. Some measurement heights proved to be strongly influenced by local effects and were not considered for the statistical analysis (black crosses in Figure 4). At VT 5 the lowest measurement height was affected by a tall building very close by, which was not considered during the planning of the measurement layout. The measurement heights of the WC are evenly spaced at a distance of 20 m, with the lowest height at 365 m asl. For comparison with the VTs, the height levels of the WC closest to the corresponding VT common height levels are used.

4 Case study

The characteristic features of the ABL are analysed in detail with a focus on the wind field for a 24-hour period, from noon of 14 August until noon of 15 August 2017. During this period, the large-scale conditions in the investigation area are dominated by a high pressure system centred over eastern Europe and a westward propagating low pressure system with centre over Scotland (Figure 5). This is associated with weak ambient wind from the south on the first day, which turned to southwest in the course of the night of the second day. The period is generally characterised by fair weather conditions and is mostly cloud free with only few cumuli topping the CBL during daytime, as visible in the measurements of global radiation at DWD station Schnarrenberg (not shown). Changes in attenuated ceilometer backscatter occur throughout the night (not shown), which are likely related to the advection of a warmer airmass associated with the change in wind direction from south to southwest.

4.1 Thermal stratification

Potential temperature profiles in the ABL from radiosoundings and the MWR (Figure 6) show that at the beginning of the investigated period the CBL is well developed, reaching up to 1900 m asl. A nocturnal SBL starts to form shortly before sunset at around 18:00 UTC, grows in depth and strength throughout the night and reaches up to around 1000 m asl at 3:00 UTC. By this time a strong surface inversion with a vertical gradient of 2.25 K(100 m)$^{-1}$ has built up reaching up to 700 m asl, visible in the radiosounding. Shortly after the SBL starts to form, the potential temperature in the residual layer above increases compared to daytime, which is likely due to the advection of warm airmasses. After around 7:00 UTC the potential temperature increases in the SBL due to surface heating, and the developing CBL erodes the SBL from below. The radiosounding at 8:00 UTC already shows a CBL reaching up to around 500 m asl. By around 11:00 UTC the CBL is well developed and reaches up to 1500 m asl.

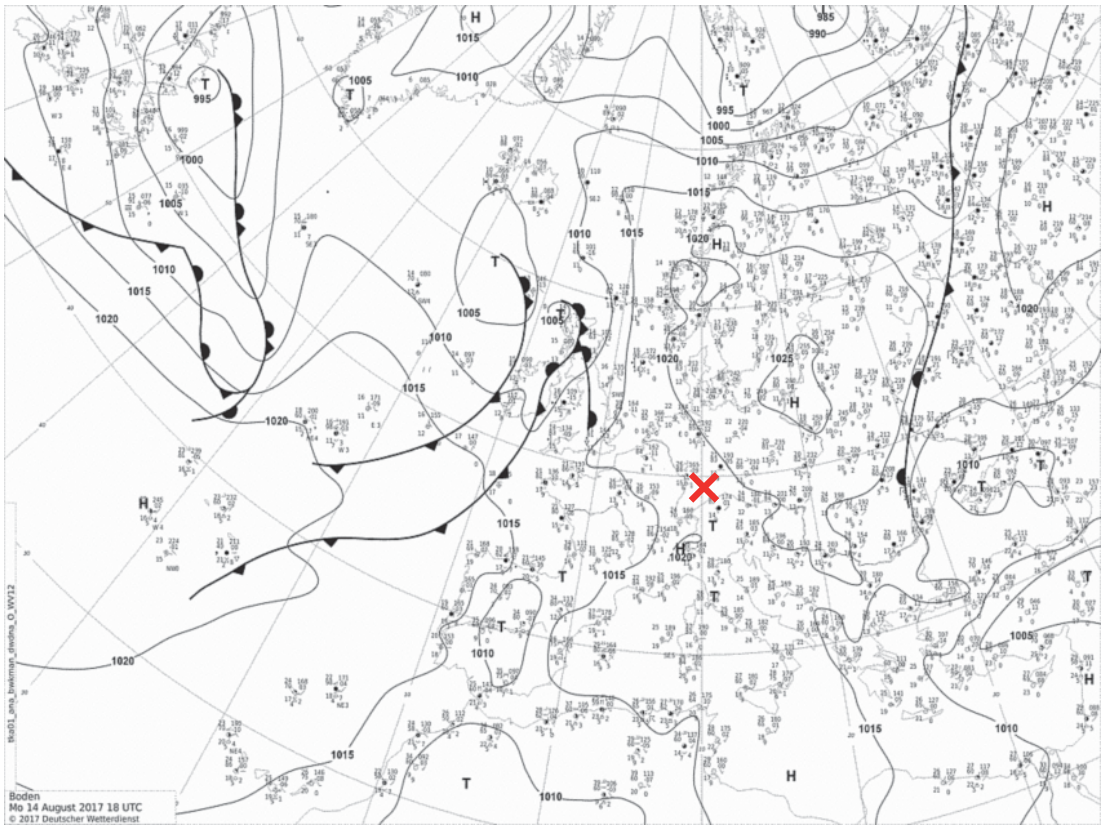

Figure 5: Surface pressure chart of Europe on 14 August 18:00 UTC. Isobars in steps of 5 hPa, the red cross marks the investigation area. (Deutscher Wetterdienst, 2017)

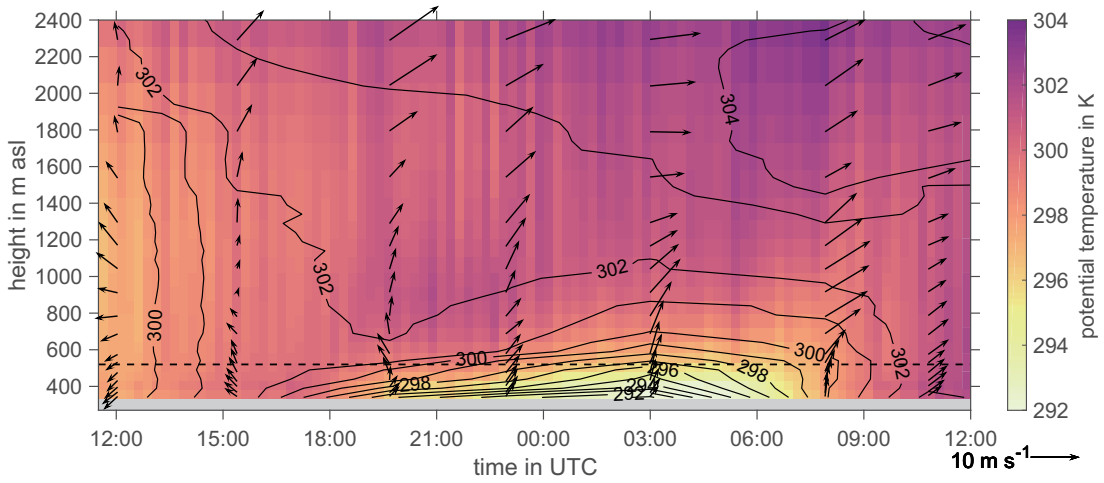

Figure 6: Evolution of potential temperature profiles from continuous MWR measurements (colour shading, at Stuttgart town hall) and from seven radiosoundings (black isolines, linearly interpolated, at Erwin-Schoettle-Platz (Figure 1)) during the case study from 14 to 15 August. Profiles of the horizontal wind from radiosoundings (arrows) are displayed at the VTs' common height levels. The dashed line marks the mean ridge height of 520 m asl. Sunset was at 18:40 UTC and sunrise at 4:15 UTC.

4.2 Temporal evolution of wind profiles

The temporal development of the wind profiles at VTs 2 and 5 in the middle of the valleys is displayed in Figure 7. In the afternoon of 14 August 2017, the CBL reaches up to the highest measurement height of the two VTs (Figures 6, 7). The wind is rather constant with height at both VTs within the CBL. The wind speed is around 4 m s^{-1} from the southeast, and the wind direction turns slightly anticyclonic with height. Shortly before sunset the wind near the surface decreases in parallel with the evolution of the SBL (Figures 6, 7). Around the same time the wind speed above and in the residual layer increases gradually downwards from the top (Figure 7), accompanied by the warm air advection (see Section 4.1).

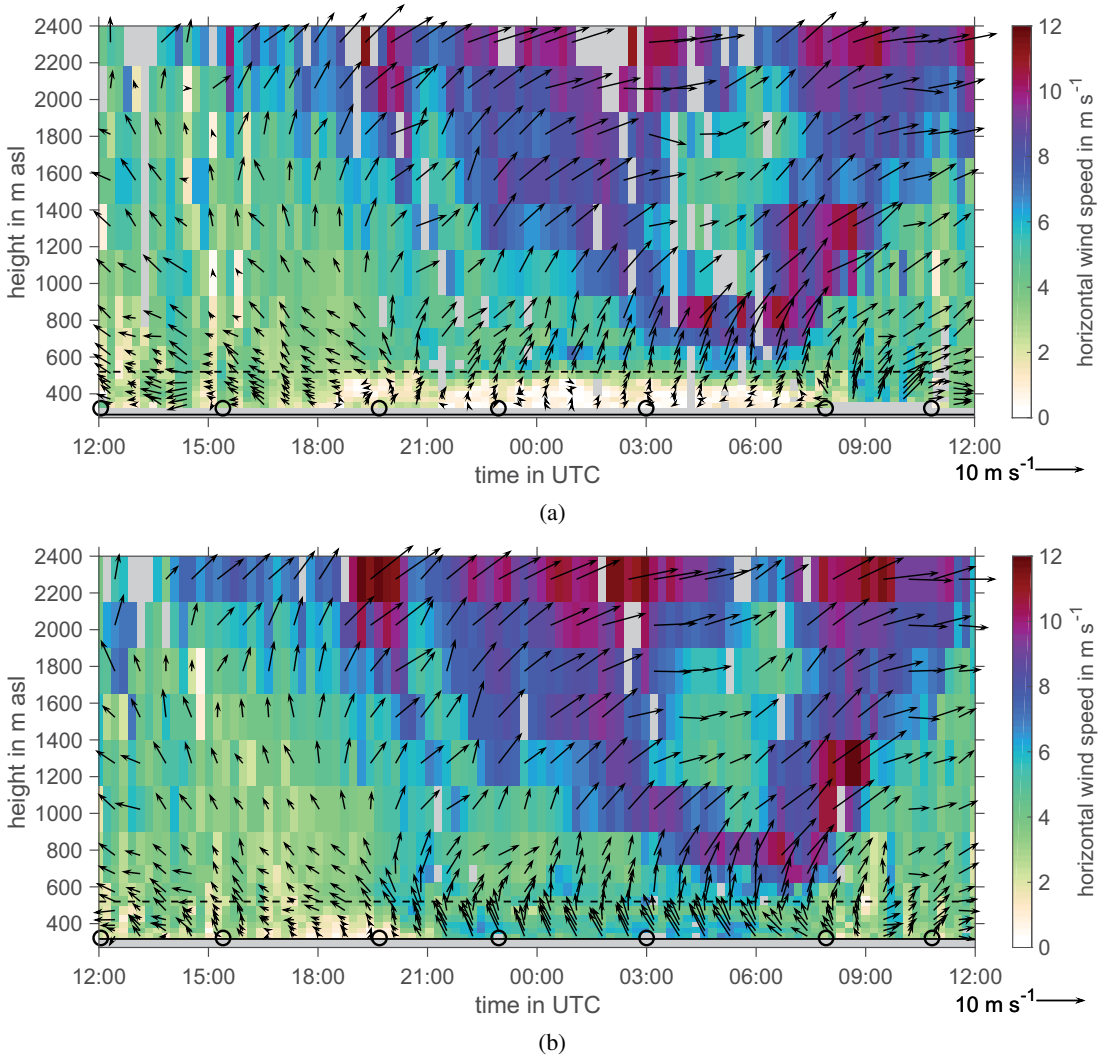

Figure 7: Evolution of the horizontal wind profiles at VT 2 (a, Stuttgart basin opening) and VT 5 (b, Neckar valley). Colour shading denotes horizontal wind speed, arrows represent horizontal wind vectors at every third measurement interval (north upwards and east to the right). Grey fields indicate no data due to filtering. Radiosonde launch times are indicated by the black circles, the dashed line marks the mean ridge height of 520 m asl and the solid black line at the bottom indicates the topographic height at the VT location. Investigation period from 12:00 UTC on 14 August until 12:00 UTC on 15 August. Sunset was at 18:40 UTC and sunrise at 4:15 UTC.

Between 23:00 UTC and 2:00 UTC a weak LLJ forms directly above ridge height, at around 600 m asl, with maximum wind speeds of 7 m s^{-1}, which is about 2 m s^{-1} stronger than the flow above at 800 m asl (Figure 7). LLJs in this height layer are frequently observed in the area around Stuttgart both in summer and winter periods (O. Kiseleva, personal communication).

Shortly after 3:00 UTC, the wind speed significantly decreases between 900 m asl and 2000 m asl at both sites. This decrease occurs rather simultaneously to the occurrence of an airmass with low backscatter observed by the ceilometer (not shown). At the same time, the wind speed increases between around 600 m asl and 800 m asl, resulting in a strong LLJ wind profile with a maximum of around 11 m s^{-1}, which is about 5 m s^{-1} faster than aloft. The LLJ stays constant until around 7:00 UTC in the morning and is clearly visible at both VTs (Figure 7), as well as in the radiosoundings (Figure 6). After about 7:00 UTC, the height of the LLJ rises up to 1300 m asl shortly before 9:00 UTC, which is likely related to the growing CBL. After 9:00 UTC, the LLJ is neither recognisable at the VT sites, nor in the last radiosounding at 10:49 UTC (Figures 6, 7). Within the growing CBL, which starts to develop at 8:00 UTC, the wind is rather constant with height at around 5 m s^{-1} from southwest.

The profiles of the wind at VT 2, VT 5 and from the radiosounding, are similar in the CBL during the day, as well as above the ridge height during the night. However, below the ridge height considerable differences between the two VTs and the radiosoundings occur during nighttime.

At the opening of the Stuttgart basin at VT 2 (see Figure 1), the wind below ridge height decreases in the evening due to the development of the SBL and the end of downward mixing of momentum (Figure 7a). The wind stays weak during the night and directions vary. In the morning after 8:00 UTC, when the CBL starts to

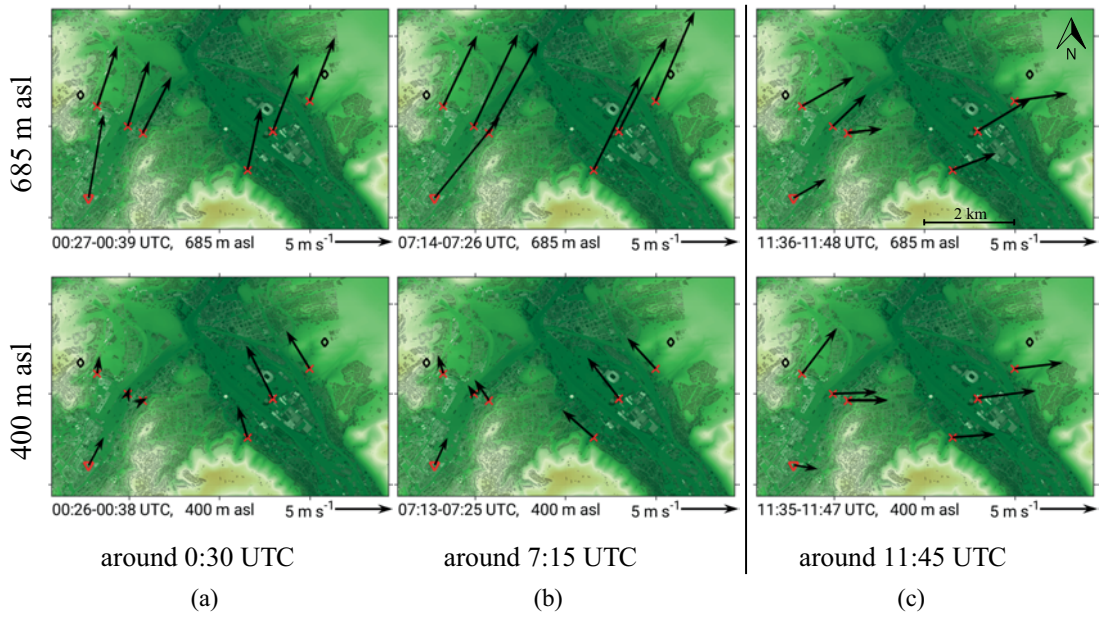

Figure 8: Spatial distribution of horizontal wind vectors at two heights in the investigation area during stable conditions around 0:30 UTC (a) and 7:15 UTC (b) and during convective conditions at around 11:45 UTC (c) on 15 August. Measurements at all VTs and the WC site are shown. Colour shading indicates terrain and building height as in Figure 1. The top figures display the wind above ridge height at approx. 685 m asl and the bottom figures show the wind below ridge height at 400 m asl. The vertical black line separates stable from convective conditions.

form, the wind becomes stronger again and the direction turns to the wind direction above, as momentum is transported downwards again.

At VT 5 in the Neckar valley (see Figure 1), the wind below the ridge height decreases around sunset similar to VT 2, but shortly after 20:00 UTC the wind starts to increase again (Figure 7b). Throughout the whole night until around 7:00 UTC in the morning, there is a strong and persistent wind of up to 7 m s^{-1}, blowing steadily from southeast. Between 21:00 UTC and 3:00 UTC the wind below ridge height is even stronger than the wind at ridge height. This corresponds to a thermally-driven down-valley wind in the Neckar valley. Once the stratification becomes unstable and a CBL starts to form at around 8:00 UTC (Figure 6), the down-valley wind weakens and eventually is replaced by southwesterly flow.

In the Stuttgart basin, the radiosoundings at Erwin-Schoettle-Platz (see Figure 1) measure wind of around 4 m s^{-1} from southwest in the SBL (Figure 6). This indicates the existence of a thermally-driven down-valley wind in the Nesenbach valley, which is penetrating into the Stuttgart basin.

4.3 Spatial differences in the wind field

In general three flow characteristics can be distinguished from the analysis of the wind profiles in Section 4.2: (i) during daytime, the wind is well mixed in the CBL down to the surface; during nighttime, (ii) an LLJ above ridge height is observed and (iii) thermally driven down-valley winds are detected in the Neckar Valley and at Erwin-Schoettle-Platz in the Stuttgart basin below the ridge height.

To investigate the spatial variability of these characteristics, horizontal sections of the wind at all VTs and the WC site are plotted at two heights, one below and one above the mean ridge height, for two time periods in the SBL and one time period in the CBL (Figure 8). The lower height level 400 m asl was chosen, as it is well below the ridge height, but high enough above the ground at all sites for not to be disturbed by local effects like buildings (Figure 4). The higher level 685 m asl was chosen, because at VT 2 and VT 5 the LLJ could be observed in this height (Figure 7) and data availability of the WC and the VTs was quite high. The horizontal sections are plotted at three times, which are chosen based on the observations at VT 2 and VT 5 (Figure 7): at around 0:30 UTC (Figure 8a), an LLJ is observed for the first time in the night and a down-valley wind occurs in the Neckar valley. At 7:15 UTC (Figure 8b) the sun has already risen and a shallow CBL starts to erode the SBL from below (Figure 6), the LLJ is most pronounced and the down-valley wind in the Neckar valley starts to weaken (Figure 7). At around 11:45 UTC (Figure 8c), both measurement heights are within the CBL (Figure 6).

At 0:30 UTC, the LLJ can be observed at all sites above the ridge height, with similar wind speed and direction, i.e. around 7 m s^{-1} from south-southwest (Figure 8a). This indicates that the LLJ is a mesoscale phenomenon in the area, independent from the local topography. Below the ridge height, a distinct down-valley wind of around 5 m s^{-1} occurs in the Neckar valley at

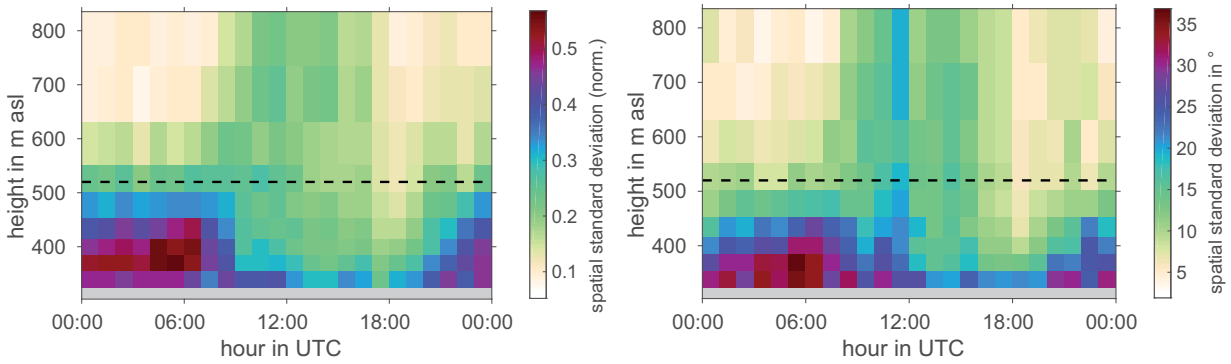

(a) (b)

Figure 9: Daily composites of the hourly spatial standard deviations of horizontal wind speed (a, normalised with the hourly mean horizontal wind speed) and wind direction (b) for the six VTs. The dashed black line indicates the mean ridge height.

VTs 4, 5 and 6. At VTs 1, 2 and 3 a weak outflow from the Stuttgart basin is visible. In the basin, the WC shows an inflow into the basin from the Nesenbach valley, which agrees with the radiosonde measurements close to the Nesenbach valley exit (Figure 6).

At 7:15 UTC, the LLJ blows strongly from southwest at all sites, with a wind speed of around $9\,\mathrm{m\,s^{-1}}$ (Figure 8b). Below the ridge height the down-valley wind in the Neckar valley is still present but slightly weaker than at 0:30 UTC. This could be related to the evolution of the CBL that starts around the same time (Figure 6). At the opening of the Stuttgart basin at VTs 1, 2 and 3, no outflow is observed but the wind increased slightly and turned to southeast, possibly influenced by the down-valley wind in the Neckar valley (Figure 8b). In the basin, an outflow from the Nesenbach valley is still visible at the WC site. During both nighttime periods, the wind below ridge height depends on the location in the valley and is independent from the wind above, i.e. they are decoupled.

At 11:45 UTC the wind is generally similar in speed and direction (westerly at around $5\,\mathrm{m\,s^{-1}}$) at all measurement locations and both heights (Figure 8c), which indicates vertical coupling by convection in the CBL.

5 Topographic influence on the wind field

The case study reveals a considerable influence of the topography on the wind field, depending on atmospheric stratification and height (Section 4). In the following the influence of the topography on the flow below ridge height is investigated statistically for the whole campaign, taking into account stratification and the ambient wind. The weather during the campaign was diverse, including several passing cyclones as well as calm, fair weather periods.

5.1 Height dependence of the topographic influence

To assess how strongly the wind at the different height levels of the VTs is influenced by the topography, the spatial variability of the wind is examined. The approach is based on the assumption that at low heights the wind at the different VT sites differs strongly due to differences of the topography surrounding the sites, while at higher levels the wind is controlled by large-scale pressure gradients and less affected by the topography, i.e. the wind is similar at all locations. To assess the spatio-temporal variability, spatial standard deviations of the hourly averaged wind speed and direction were calculated. The spatial standard deviations σ of the wind speed U for each common height level z were calculated for every hourly timestamp t over all six VTs ($i = 1, \ldots, 6$), and normalised by the mean wind speed for all VTs $\bar{U}(t, z)$:

$$\frac{\sigma(t,z)}{\bar{U}(t,z)} = \frac{\sqrt{\frac{1}{6}\sum_{i=1}^{6}\left(U_i(t,z) - \bar{U}(t,z)\right)^2}}{\bar{U}(t,z)}\,. \qquad (5.1)$$

The spatial standard deviations of the wind direction are calculated respectively (without normalisation), using a method proposed by Yamartino (1984). The small sample size of 6 VTs used for the calculation of the standard deviation may lead to some uncertainty. The daily composites, i.e. means for each hour of the day, of the normalised spatial standard deviations of wind speed and spatial standard deviations of wind direction are displayed in Figure 9.

The daily composites of the spatial standard deviations show two distinct regimes, which indicate a dependency on stratification: between around 9:00 UTC and 20:00 UTC, i.e. mainly during daytime, medium values are found at all levels, and between around 20:00 UTC and 9:00 UTC, i.e. mainly during nighttime, high spatial standard deviations occur below the ridge height, with low values above.

The moderate values during the day are probably related to the small sample size (4–5 values, each derived from 10 s measurement periods) used for the calculation of the hourly means. Especially during periods of enhanced turbulence, like in the CBL, the hourly means calculated from these short periods and few samples may not represent the mean wind very well (see

Section 3.3) and thus induce some spatial variability. This may be the reason for the moderate values of the (normalised) spatial standard deviations during daytime (Figure 9).

During nighttime, the spatial standard deviations decrease with height and reach a minimum at around 685 m asl (Figure 9), i.e. the flow below ridge height is influenced by the topography while the wind above is less influenced and more similar at all locations, this is in line with the findings of the case study (Section 4). Based on these results, two height levels are determined for the further statistical analysis of the wind. The height level at 400 m asl is chosen as the height where the wind is strongly influenced by the topography (hereafter low-level wind). 685 m asl is chosen as the height level which reflects the ambient wind and which is mostly unaffected by the topography.

5.2 Relationship between ambient and low-level wind

The analysis in Section 5.1 indicates that the topographic influence on the low-level wind depends on the atmospheric stratification. To get information on the stratification of the ABL regarding both thermal and dynamical effects, the bulk Richardson number (BRN) can be used. The BRN is calculated as defined by Stull (1988):

$$BRN = \frac{g\,\Delta\theta_v\,\Delta z}{\theta_v\,\left[(\Delta u)^2 + (\Delta v)^2\right]}\,, \tag{5.2}$$

with the gravitational acceleration g. The differences in virtual potential temperature from the MWR, $\Delta\theta_v$, and the wind components, Δu and Δv, are calculated between 685 m asl and 400 m asl, i.e. the layer depth Δz is 285 m. The virtual potential temperature θ_v is the mean of the two levels. Negative BRNs indicate statically unstable conditions. For positive BRNs, the conditions are statically stable and turbulence is suppressed by the stratification, but can be produced by vertical wind shear. The flow is assumed to become dynamically unstable for BRNs smaller than a critical value and to remain stable for BRNs larger than the critical value.

To assess how the influence of the topography on the low-level wind depends on the stratification, the median absolute deviation of the low-level wind direction from the along valley axes is plotted in Figure 10, in dependence of the BRN. For BRNs below 1 the average absolute deviation from the valley axis is around 45°, which indicates little dependence of the flow on the valley direction. For BRNs above 2 the deviations are mainly between 10° and 20°, which means that the flow is mostly aligned with valley axis. Between BRNs of 1 and 2 the flow conditions change between the two regimes. In particular for VT 5, a sharp decrease in the mean absolute deviation occurs for a BRN value of 1.25. VT 5 lies in the centre of the Neckar valley whose shape and axis is more pronounced than in the Stuttgart basin or the

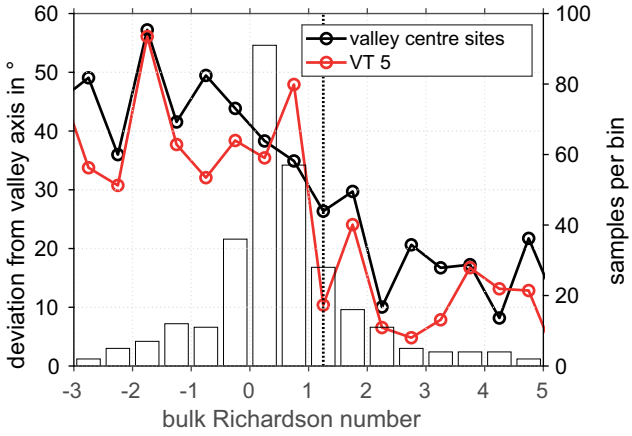

Figure 10: Absolute deviation of the low-level wind direction from the valley axis (up- and down-valley direction) depending on the BRN. Median (lines) of the deviation at the valley centre sites (VT 2, VT 5, WC) and at VT 5, for BRN bins with width 0.5. The vertical dotted line marks a BRN of 1.25. The histogram shows the number of samples per BRN bin at VT 5.

basin opening and thus allows for a more distinct evolution of thermally driven circulations and a clearer impact of the topography on the flow. This is likely the reason why the decrease in the median absolute deviation is less pronounced when averaging over all valley centre sites (VT 5, VT 2 and WC).

In the next step, the dependency of the low-level wind direction on the ambient wind direction is investigated for different BRNs (Figure 11). For negative BRNs the low-level wind directions are very similar to the ambient wind direction at all sites and no effects of the topography are visible (beige circles in Figure 11). This indicates that vertical mixing due to buoyancy-driven turbulence, i.e. convection, couples the low-level and the ambient flow. These cases have on the average a deviation from valley axis of 45° (Figure 10).

For BRNs between 0 and 1.25 (green circles in Figure 11), the wind directions are generally similar at both height levels, but the low-level wind vectors are rotated cyclonically and begin to turn towards the down-valley direction, which indicates reduced vertical mixing compared to the cases with negative BRNs. The cyclonic rotation is likely caused by surface friction slowing down the wind towards the surface, which leads to a reduction of the Coriolis force. For this BRN range, the main influence on the low-level wind direction is still the ambient wind, which means that momentum is transported downward by shear-driven turbulence, however, some influences from the topography are also visible. In some cases also the down-valley winds might be caused or enhanced by pressure-driven channelling, but the visible effects on the wind direction relation in these cases are the same as for thermally driven down-valley winds and therefore the underlying forces cannot be distinguished. For BRNs larger than 1.25, the wind directions at VT 5 largely coincide with the down-valley direction (Figure 11b). For VT 2 and the WC (Figure 11a,b) the

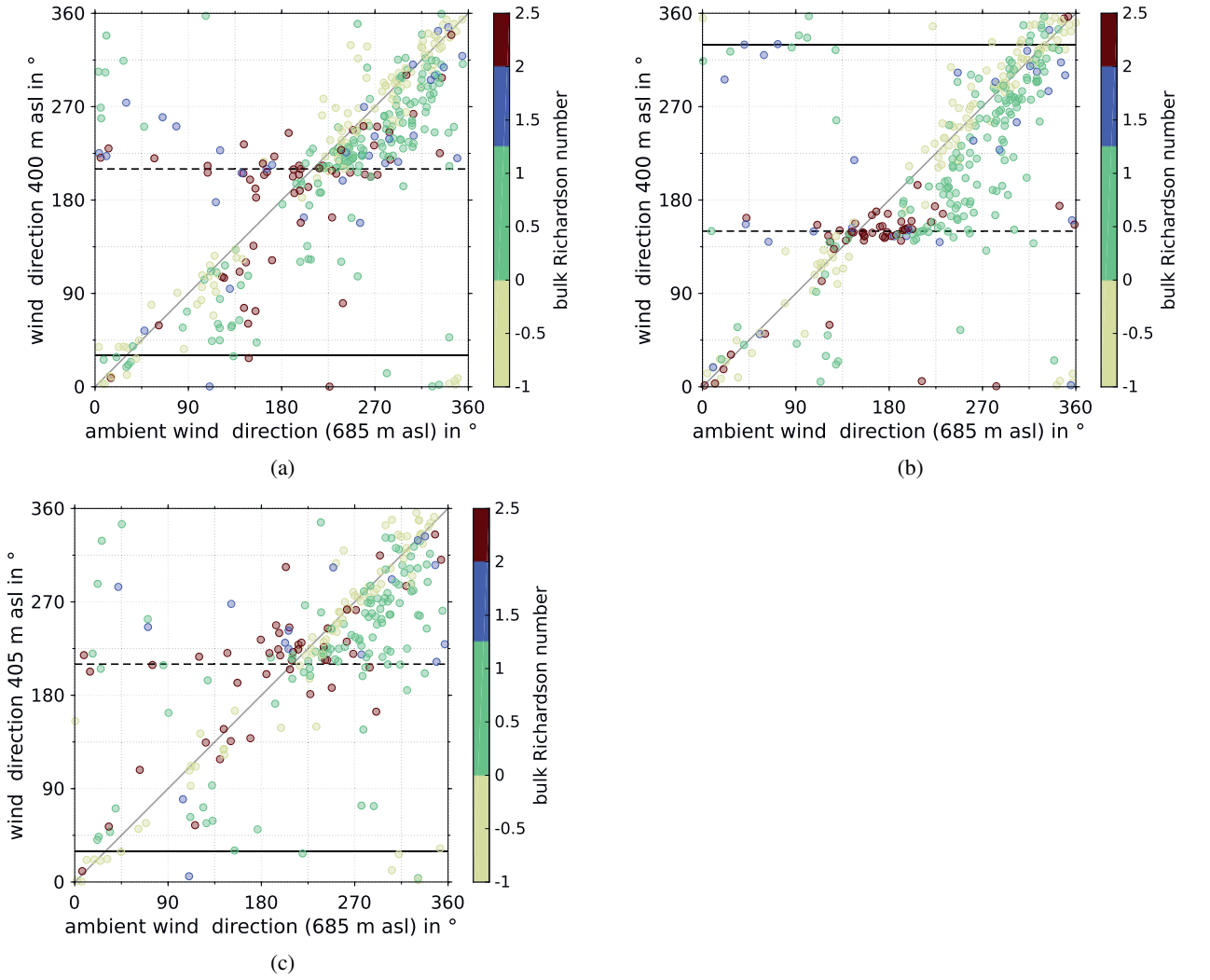

Figure 11: Relationship between the wind directions of ambient (x-axis) and low-level wind (y-axis) at VT 2 (a, Stuttgart basin opening), VT 5 (b, Neckar valley) and the WC site (c, Stuttgart basin centre). The colours denote the bulk Richardson number (BRN, Eq. 5.2). The dashed horizontal line indicates the down-valley direction of the Neckar valley and the Stuttgart basin, the solid horizontal line marks the up-valley direction. Markers on the grey diagonal line indicate that the wind directions are the same at both levels.

low-level wind directions for BRNs greater than 1.25 are also mostly scattered around the down-valley direction, although the spread is larger than for VT5. This is possibly related to the shape of the Stuttgart basin and the much smaller dimension of the Nesenbach Valley, in comparison to the relatively long, deep and straight Neckar Valley and agrees with the sharp decrease of the median absolute deviations of the wind direction from the valley for BRNs of 1.25 at VT 5 (Figure 10).

Overall, turbulent downward momentum transport seems to be the dominating influence at all sites for BRNs below 1.25. For values larger than 1.25 the topographic influence becomes dominant and down-valley flows are prevailing. Thus, we identify 1.25 as the critical value for the BRN, above which the flow is dynamically stable, i.e. decoupled, and below which it is dynamically unstable, i.e. coupled.

5.3 Spatial distribution of the low-level wind

Using the critical value of the BRN found in Section 5.2 the spatial distribution of the low-level wind is examined further using wind roses at the six VTs and the WC site. For dynamically unstable conditions (BRN < 1.25) the wind roses generally show a similar wind distribution throughout the area at all sites in both 400 m asl and 685 m asl (not shown), as expected from the previous analysis.

For dynamically stable conditions (BRN > 1.25) there are considerable differences between the lower and the upper level. While at the upper level, the wind roses at all sites are very similar and indicate prevailing westerly direction (not shown), the wind roses at 400 m asl strongly depend on the site location (Figure 12): in the Stuttgart basin (WC) and at the opening of the basin (VTs 1,

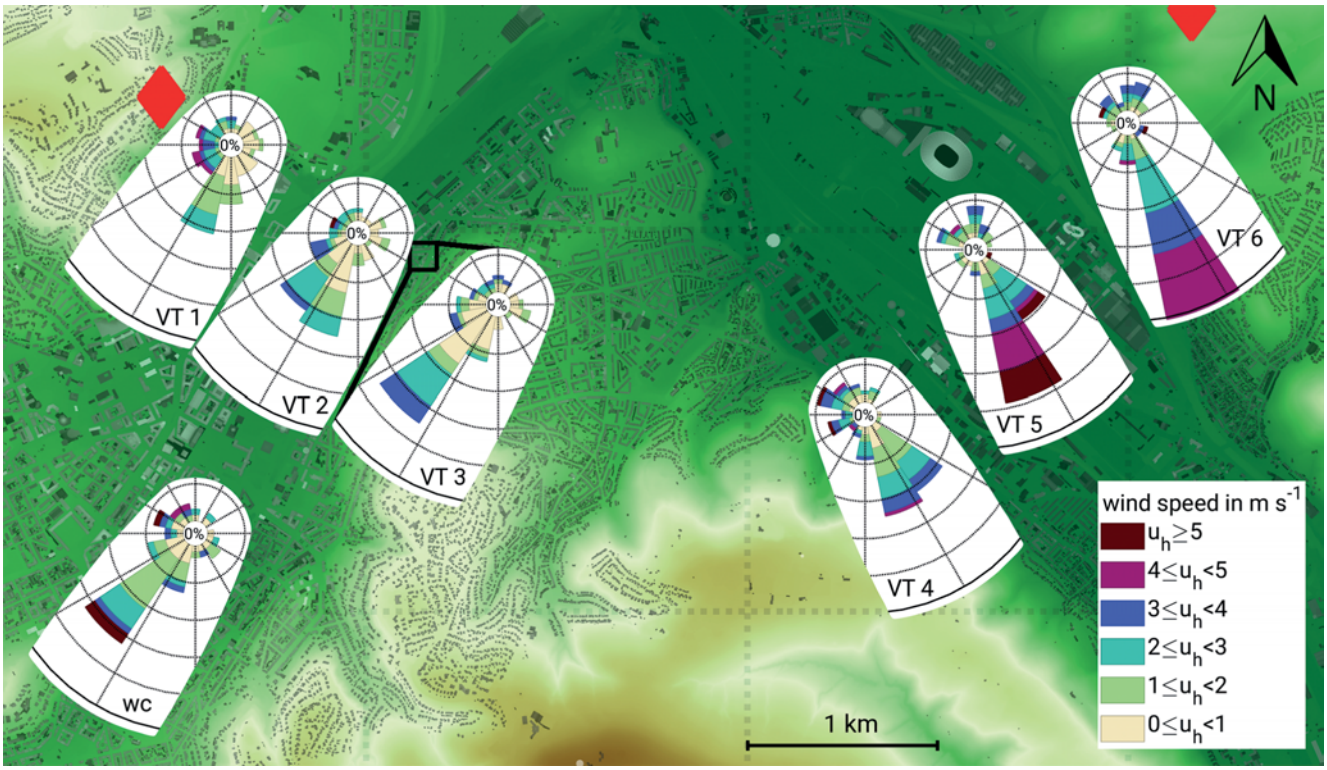

Figure 12: Wind roses for dynamically stable conditions (BRN ≥ 1.25) at 400 m asl displayed at the different sites in the Stuttgart basin and in the Neckar valley. Wind rose frequency grid is in 10 % steps. The wind rose of VT 3 is slightly shifted to the right as indicated by the black lines. Red diamonds indicate positions of WTX and HYB. Terrain height and buildings as in Figure 1.

2 and 3) weak (< 3 m s^{-1}) southwesterly wind prevails, while in the Neckar valley (VTs 4, 5 and 6) moderate to strong (up to 5 m s^{-1}) south-southeasterly wind dominates. The dominating wind direction at all locations is down-valley, which indicates the regular occurrence of thermally driven circulations in the area for dynamically stable conditions. The down-valley winds are most pronounced in the Neckar valley. At the WC site in the middle of the Stuttgart basin the down-valley flow is stronger than at the basin opening, which is likely related to a down-valley wind flowing out of the Nesenbach valley into the basin (see Figure 1). At the opening of the basin at VTs 1, 2 and 3, the occurring winds are comparatively weak, which is probably due to the shape of the basin, not allowing stronger down-valley winds to develop (Figure 12). At VTs 1, 2 and 3 the flow slightly diverges, possibly resulting from the widening of the valley towards the Neckar valley. Besides the outflow from the Stuttgart basin, some cases with moderate southwesterly to northwesterly wind are found at VT 1, which are much less frequent than the outflow cases. This could possibly be related to thermally driven downslope flows forming on the slopes northwest of VT 1. At VT 4, some cases with westerly wind occur which could be related to the outflow of the Stuttgart basin passing over the shallow plateau between VT 3 and VT 4.

6 Summary and conclusions

In the framework of the project [UC]^2 the flow in the ABL over Stuttgart, a major city in mountainous terrain in southwestern Germany, was observed using dual-Doppler lidar measurements in summer 2017. Vertical profiles of the horizontal wind, so-called virtual towers (VTs) were retrieved at six positions at the opening of the Stuttgart basin and in the Neckar valley with discrete measurement heights between 30–2000 m agl. Additionally, a third profiling Doppler lidar measured wind profiles in the Stuttgart basin and a microwave radiometer was used to obtain information on atmospheric stratification. The data were used to investigate the mesoscale flow characteristics in the urban ABL over a complex topography characterised by a basin-shaped valley (Stuttgart basin) which opens to the relatively straight Neckar valley.

The main findings of this study are:

1. As the VT technique has so far not been used to study mesoscale flow structures over mountainous urban terrain, we first demonstrated that it is a suitable method to provide high-quality wind profile information over complex terrain, given that a sophisticated scan strategy and intense processing and quality control are performed. The radial velocity measurements

from each Doppler lidar corresponding to VTs are selected using geometric considerations and the raw radial velocity data is filtered in three steps using a maximum radial velocity threshold, a minimum signal-to-noise ratio threshold and an outlier filter based on the median absolute deviation. 81 % of the raw data remained after applying these filtering steps. The radial velocities are averaged over the 10 s measurement intervals at each measurement height of the VTs and wind is calculated, if both lidars have a minimum data availability per interval. Finally 89 % of the initial 10 s measurement intervals passed the quality checks and were used for the analysis. The resulting wind profiles qualitatively show a good agreement with other wind measurements of the profiling lidar and radiosondes.

2. In order to identify the flow patterns occurring in the urban ABL, we analysed a 24-hour case study under fair weather conditions. While the horizontal flow is rather constant with height in the ABL under convective conditions, distinct differences occur during nighttime under stable conditions below the ridge height. A pronounced down-valley wind is observed in the Neckar valley and in the Stuttgart basin near the exit of the Nesenbach valley. Above the ridge height the flow is spatially homogeneous throughout the area and a low-level jet is observed in the second half of the night. The case study indicates that the flow below and above ridge height is coupled under convective conditions and decoupled under stable conditions, which allows the development of thermally driven flows.

3. To generalise the dependence of the flow on topography and stratification found in the case study, we investigate all available days and thus consider all kinds of large-scale conditions. In order to quantify which measurement heights are affected by the topography, we calculated spatial standard deviations of the hourly averaged wind speed and direction and find a considerable topographic influence below the ridge height during nighttime, while the topographic influence above the ridge height is much lower. During the day, spatial standard deviations are smaller and no clear topographic influence can be detected. Based on this analysis we choose two measurement heights for the further investigation: one level below ridge height, where the wind is strongly influenced by the topography, and one level above ridge height which is assumed to reflect the ambient wind.

   The relationship between the low-level and ambient wind strongly depends on the bulk Richardson number (BRN). We identify a critical BRN of 1.25 for the area. For BRNs smaller than the critical value, the flow above and below ridge height are coupled. If the BRN is larger than 1.25 (dynamically stable), mainly down-valley winds are observed in the Neckar valley and in the Stuttgart basin and an outflow is detected at the opening of the Stuttgart basin, independent of the ambient wind direction. There is evidence for a few cases where pressure-driven channelling causes up-valley flow in the Neckar valley. The relationship between the low-level and ambient wind is somewhat less clear in the Stuttgart basin and at the basin opening compared to the Neckar valley, which is likely related to the different dimensions and shapes of the valleys. Wind roses for dynamically stable conditions nicely demonstrate the dependence of the flow on the topography at the different sites.

This study shows that VTs from dual-Doppler lidar measurements are a powerful method to investigate the wind field over complex terrain. Depending on the research interest, arrays of VTs can be used for temporal and spatial investigation of mesoscale circulations or microscale flow patterns. A high spatial coverage can be achieved using many VTs, or few VTs with a higher temporal resolution can be used to obtain more reliable statistics. The possibilities of the VT method are only limited by geometric requirements and the availability of atmospheric scatterers and enable measurements in the ABL in regions that are difficult to access with in situ measurements, like urban terrain. At the expense of the vertical coverage, the horizontal resolution of the wind field can be further increased by performing synchronous coplanar horizontal scans with multiple lidars. Adler et al. (2020) used this approach to identify structures in the horizontal flow field over Stuttgart and to detect the displacement of convective cells in the ABL. The detected down-valley winds in the Nesenbach valley and outflow at the opening of the Stuttgart basin result in a ventilation of the basin, which is likely to have a considerable influence on the air quality in the city by removing pollutants. The effects of the ventilation by down-valley winds could be further investigated by combining the VT wind measurements with pollutant measurements. The dependence of the air quality in the Stuttgart basin on the conditions in the ABL will be examined in further studies.

Acknowledgements

The German Federal Ministry of Education and Research (BMBF) funded the project under grant 01LP1602 G within the research programme [UC]^2. We would like to thank Andreas Wieser and the whole team from IMK for the instrument installation and the conduction of the campaign. Further we would like to thank our project partners Meinolf Kossmann and the DWD for radiosonde, ceilometer and near-surface data, Rayk Rinke from the city of Stuttgart and the DLR for topographic data. We thank the three anonymous reviewers, whose comments helped to improve the quality of this publication. Thanks a lot to the city of Stuttgart and to the winery Wöhrwag for kindly providing suitable sites for the instrument setup.

References

Adler, B., N. Kalthoff, O. Kiseleva, 2020: Detection of structures in the horizontal wind field over complex terrain using coplanar doppler lidar scans. – Meteorol. Z. **29**, 467–481, DOI: 10.1127/metz/2020/1031.

Allwine, K.J., J.H. Shinn, G.E. Streit, K.L. Clawson, M. Brown, 2002: Overview of URBAN 2000: A multiscale field study of dispersion through an urban environment. – Bull. Amer. Meteor. Soc. **83**, 521–536, DOI: 10.1175/1520-0477(2002)083<0521:OOUAMF>2.3.CO;2.

Barlow, J.F., 2014: Progress in observing and modelling the urban boundary layer. – Urb. Climate **10**, 216–240, DOI: 10.1016/j.uclim.2014.03.011.

Bingöl, F., J. Mann, D. Foussekis, 2009: Conically scanning lidar error in complex terrain. – Meteorol. Z. **18**, 189–195, DOI: 10.1127/0941-2948/2009/0368.

Calhoun, R., R. Heap, M. Princevac, R. Newsom, H. Fernando, D. Ligon, 2006: Virtual towers using coherent Doppler lidar during the Joint Urban 2003 dispersion experiment. – J. Appl. Meteor. Climatol. **45**, 1116–1126, DOI: 10.1175/JAM2391.1.

Choukulkar, A., W.A. Brewer, S.P. Sandberg, A. Weickmann, T.A. Bonin, R.M. Hardesty, J.K. Lundquist, R. Delgado, G.V. Iungo, R. Ashton, M. Debnath, L. Bianco, J.M. Wilczak, S. Oncley, D. Wolfe, 2017: Evaluation of single and multiple Doppler lidar techniques to measure complex flow during the XPIA field campaign. – Atmos. Meas. Tech. **10**, 247–264, DOI: 10.5194/amt-10-247-2017.

Collier, C.G., F. Davies, K.E. Bozier, A.R. Holt, D.R. Middleton, G.N. Pearson, S. Siemen, D.V. Willetts, G.J. Upton, R.I. Young, 2005: Dual-Doppler lidar measurements for improving dispersion models. – Bull. Amer. Meteor. Soc. **86**, 825–838, DOI: 10.1175/BAMS-86-6-825.

Crewell, S., U. Löhnert, 2007: Accuracy of boundary layer temperature profiles retrieved with multifrequency multiangle microwave radiometry. – IEEE Trans. Geosci. Remote Sens. **45**, 2195–2201, DOI: 10.1109/TGRS.2006.888434.

Damian, T., A. Wieser, K. Träumner, U. Corsmeier, C. Kottmeier, 2014: Nocturnal low-level jet evolution in a broad valley observed by dual doppler lidar. – Meteorol. Z. **23**, 305–313, DOI: 10.1127/0941-2948/2014/0543.

Deutscher Wetterdienst, 2017: wetter3.de, DWD Analyse-Archiv. – http://www1.wetter3.de/archiv_dwd_dt.html, accessed: 2018-09-21.

Giovannini, L., L. Laiti, S. Serafin, D. Zardi, 2017: The thermally driven diurnal wind system of the Adige Valley in the Italian Alps. – Quart. J. Roy. Meteor. Soc. **143**, 2389–2402, DOI: 10.1002/qj.3092.

Kalthoff, N., H.J. Binder, M. Kossmann, R. Vögtlin, U. Corsmeier, F. Fiedler, H. Schlager, 1998: Temporal evolution and spatial variation of the boundary layer over complex terrain. – Atmos. Env. **32**, 1179–1194, DOI: 10.1016/S1352-2310(97)00193-3.

Kalthoff, N., B. Adler, A. Wieser, M. Kohler, K. Träumner, J. Handwerker, U. Corsmeier, S. Khodayar, D. Lambert, A. Kopmann, N. Kunka, G. Dick, M. Ramatschi, J. Wickert, C. Kottmeier, 2013: KITcube–a mobile observation platform for convection studies deployed during HyMeX. – Meteorol. Z. **22**, 633–647, DOI: 10.1127/0941-2948/2013/0542.

Kiseleva, O., B. Adler, N. Kalthoff, M. Kohler, A. Wieser, N. Wittkamp, 2019: Data set of meteorological observations (wind, temperature, humidity) collected from a microwave radiometer and lidar measurements during four intensive observations periods in 2017 and 2018 in Stuttgart, Germany, under the BMBF Programme 'Urban Climate Under Change' [UC]2). – Karlsruher Institut für Klimatologie, published online. DOI: 10.5445/IR/1000093534.

Klaus, D., S. Mertes, A. Siegmund, 2003: Coherences between upper air flow and channelling mechanism in the Baar Basin. – Meteorol. Z. **12**, 217–227, DOI: 10.1127/0941-2948/2003/0012-0217.

Kossmann, M., R. Vögtlin, U. Corsmeier, B. Vogel, F. Fiedler, H.J. Binder, N. Kalthoff, F. Beyrich, 1998: Aspects of the convective boundary layer structure over complex terrain. – Atmos. Env. **32**, 1323–1348, DOI: 10.1016/S1352-2310(97)00271-9.

Kuttler, W., D. Dütemeyer, A.B. Barlag, 1998: Influence of regional and local winds on urban ventilation in Cologne, Germany. – Meteorol. Z. **7**, 77–87, DOI: 10.1127/metz/7/1998/77.

Lareau, N.P., E. Crosman, C.D. Whiteman, J.D. Horel, S.W. Hoch, W.O. Brown, T.W. Horst, 2013: The persistent cold-air pool study. – Bull. Amer. Meteor. Soc. **94**, 51–63, DOI: 10.1175/BAMS-D-11-00255.1.

Löhnert, U., S. Crewell, 2003: Accuracy of cloud liquid water path from ground-based microwave radiometry 1. Dependency on cloud model statistics. – Radio Sci. **38**, 8041, DOI: 10.1029/2002RS002654.

Löhnert, U., D. Turner, S. Crewell, 2009: Ground-based temperature and humidity profiling using spectral infrared and microwave observations. Part I: Simulated retrieval performance in clear-sky conditions. – J. Appl. Meteor. Climatol. **48**, 1017–1032, DOI: 10.1175/2008JAMC2060.1.

Machiwal, D., M.K. Jha, 2012: Hydrologic time series analysis: theory and practice. – Springer Science & Business Media, Dordrecht, 301.

Maronga, B., G. Gross, S. Raasch, S. Banzhaf, R. Forkel, W. Heldens, F. Kanani-Sühring, A. Matzarakis, M. Mauder, D. Pavlik, J. Pfafferott, S. Schubert, G. Seckmeyer, H. Sieker, K. Winderlich, 2019: Development of a new urban climate model based on the model PALM – Project overview, planned work, and first achievements. – Meteorol. Z. **28**, 105–119, DOI: 10.1127/metz/2019/0909.

Mayer, H., 1999: Air pollution in cities. – Atmos. Env. **33**, 4029–4037, DOI: 10.1016/S1352-2310(99)00144-2.

Newman, J.F., T.A. Bonin, P.M. Klein, S. Wharton, R.K. Newsom, 2016: Testing and validation of multi-lidar scanning strategies for wind energy applications. – Wind Energy **19**, 2239–2254, DOI: 10.1002/we.1978.

Newsom, R.K., D. Ligon, R. Calhoun, R. Heap, E. Cregan, M. Princevac, 2005: Retrieval of microscale wind and temperature fields from single- and dual-Doppler lidar data. – J. Appl. Meteor. **44**, 1324–1345, DOI: 10.1175/JAM2280.1.

Pauscher, L., N. Vasiljevic, D. Callies, G. Lea, J. Mann, T. Klaas, J. Hieronimus, J. Gottschall, A. Schwesig, M. Kühn, M. Courtney, 2016: An inter-comparison study of multi- and DBS lidar measurements in complex terrain. – Remote Sens. **8**, 782, DOI: 10.3390/rs8090782.

Piringer, M., K. Baumann, 1999: Modifications of a valley wind system by an urban area–experimental results. – Meteor. Atmos. Phys. **71**, 117–125, DOI: 10.1007/s007030050049.

Rendón, A.M., J.F. Salazar, V. Wirth, 2020: Daytime air pollution transport mechanisms in stable atmospheres of narrow versus wide urban valleys. – Env. Fluid Mech. **20**, 1101–1118, DOI: 10.1007/s10652-020-09743-9.

Röhner, L., K. Träumner, 2013: Aspects of convective boundary layer turbulence measured by a dual-Doppler lidar system. – J. Atmos. Ocean. Technol. **30**, 2132–2142, DOI: 10.1175/JTECH-D-12-00193.1.

Rose, T., S. Crewell, U. Löhnert, C. Simmer, 2005: A network suitable microwave radiometer for operational monitor-

ing of the cloudy atmosphere. – Atmos. Res. **75**, 183–200, DOI: 10.1016/j.atmosres.2004.12.005.

Rothermel, J., C. Kessinger, D.L. Davis, 1985: Dual-Doppler lidar measurement of winds in the JAWS experiment. – J. Atmos. Ocean. Technol. **2**, 138–147, DOI: 10.1175/1520-0426(1985)002<0138:DDLMOW>2.0.CO;2.

Scherer, D., F. Ament, S. Emeis, U. Fehrenbach, B. Leitl, K. Scherber, C. Schneider, U. Vogt, 2019a: Three-dimensional observation of atmospheric processes in cities. – Meteorol. Z. **28**, 121–138, DOI: 10.1127/metz/2019/0911.

Scherer, D., F. Antretter, S. Bender, J. Cortekar, S. Emeis, U. Fehrenbach, G. Gross, G. Halbig, J. Hasse, B. Maronga, S. Raasch, K. Scherber, 2019b: Urban climate under change [UC]^2–a national research programme for developing a building-resolving atmospheric model for entire city regions. – Meteorol. Z. **28**, 95–104, DOI: 10.1127/metz/2019/0913.

Stawiarski, C., K. Träumner, C. Knigge, R. Calhoun, 2013: Scopes and challenges of dual-Doppler lidar wind measurements–an error analysis. – J. Atmos. Ocean. Technol. **30**, 2044–2062, DOI: 10.1175/JTECH-D-12-00244.1.

Steyn, D.G., J. Bottenheim, R. Thomson, 1997: Overview of tropospheric ozone in the Lower Fraser Valley, and the Pacific'93 field study. – Atmos. Env. **31**, 2025–2035, DOI: 10.1016/S1352-2310(97)00018-6.

Steyn, D.G., S.F.J. De Wekker, M. Kossmann, A. Martilli, 2013: Boundary layers and air quality in mountainous terrain. – In: Chow, F.K., S.F. De Wekker, B.J. Snyder (Eds.): Mountain Weather Research and Forecasting: Recent Progress and Current Challenges. – Springer Netherlands, Dordrecht, 261–289.

Stull, R.B., 1988: An introduction to boundary layer meteorology, volume 9. – Kluwer Academic Publishers, Dordrecht, 177.

Träumner, K., T. Damian, C. Stawiarski, A. Wieser, 2015: Turbulent structures and coherence in the atmospheric surface layer. – Bound.-Layer Meteor. **154**, 1–25, DOI: 10.1007/s10546-014-9967-6.

Wanner, H., J.A. Hertig, 1984: Studies of urban climates and air pollution in switzerland. – J. Climate Appl. Meteor. **23**, 1614–1625, DOI: 10.1175/1520-0450(1984)023<1614:SOUCAA>2.0.CO;2.

Werner, C., 2005: Doppler wind lidar. – In: Weitkamp, E. (Ed.): Lidar: Range-Resolved Optical Remote Sensing of the Atmosphere. – Springer New York, New York, 325–354, DOI: 10.1007/b106786.

Yamartino, R.J., 1984: A Comparison of Several "Single-Pass" Estimators of the Standard Deviation of Wind Direction. – J. Climate Appl. Meteor. **23**, 1362–1366, DOI: 10.1175/1520-0450(1984)023<1362:ACOSPE>2.0.CO;2.